SCIENCE CHINA
Physics, Mechanics & Astronomy

•Article•
Editor's Focus

April 2022 Vol. 65 No. 4: 247462
https://doi.org/10.1007/s11433-021-1826-1

Editor's Focus

Orbital ordering and fluctuations in a kagome superconductor CsV_3Sb_5

DianWu Song[1†], LiXuan Zheng[1†], FangHang Yu[1], Jian Li[1], LinPeng Nie[1], Min Shan[1], Dan Zhao[1], ShunJiao Li[1], BaoLei Kang[1], ZhiMian Wu[1], YanBing Zhou[1], KuangLv Sun[1], Kai Liu[1], XiGang Luo[1,2], ZhenYu Wang[2], JianJun Ying[2], XianGang Wan[3,6], Tao Wu[1,2,4,6*], and XianHui Chen[1,2,4,5,6*]

[1] *Hefei National Laboratory for Physical Sciences at the Microscale, University of Science and Technology of China, Hefei 230026, China;*
[2] *CAS Key Laboratory of Strongly-coupled Quantum Matter Physics, Department of Physics, University of Science and Technology of China, Hefei 230026, China;*
[3] *National Laboratory of Solid State Microstructures and School of Physics, Nanjing University, Nanjing 210093, China;*
[4] *CAS Center for Excellence in Superconducting Electronics (CENSE), Shanghai 200050, China;*
[5] *CAS Center for Excellence in Quantum Information and Quantum Physics, Hefei 230026, China;*
[6] *Collaborative Innovation Center of Advanced Microstructures, Nanjing University, Nanjing 210093, China*

Received November 20, 2021; accepted December 2, 2021; published online February 24, 2022

Recently, competing electronic instabilities, including superconductivity and density-wave-like order, have been discovered in vanadium-based kagome metals AV_3Sb_5 (A = K, Rb, Cs) with a nontrivial band topology. This finding stimulates considerable interest to study the interplay of these competing electronic orders and possible exotic excitations in the superconducting state. Here, we performed ^{51}V and ^{133}Cs nuclear magnetic resonance (NMR) measurements on a CsV_3Sb_5 single crystal to clarify the nature of density-wave-like transition in these kagome superconductors. A first-order structural transition is unambiguously revealed below $T_s \sim 94$ K by observing the sudden splitting of Knight shift in ^{51}V NMR spectrum. Moreover, combined with ^{133}Cs NMR spectrum, the present result confirms a three-dimensional structural modulation. By further analyzing the anisotropy of Knight shift and $1/T_1T$ at ^{51}V nuclei, we proposed that the orbital order is the primary electronic order induced by the first-order structural transition, which is supported by further analysis on electric field gradient at ^{51}V nuclei. In addition, the evidence for possible orbital fluctuations is also revealed above T_s. The present work sheds light on a rich orbital physics in kagome superconductors AV_3Sb_5.

kagome superconductors, density-wave-like order, nuclear magnetic resonance, orbital order

PACS number(s): 74.25.Nf, 74.90.+n, 74.20.Mn, 76.60.Cq

Citation: D. W. Song, L. X. Zheng, F. H. Yu, J. Li, L. P. Nie, M. Shan, D. Zhao, S. J. Li, B. L. Kang, Z. M. Wu, Y. B. Zhou, K. L. Sun, K. Liu, X. G. Luo, Z. Y. Wang, J. J. Ying, X. G. Wan, T. Wu, and X. H. Chen, Orbital ordering and fluctuations in a kagome superconductor CsV_3Sb_5, Sci. China-Phys. Mech. Astron. **65**, 247462 (2022), https://doi.org/10.1007/s11433-021-1826-1

*Corresponding authors (Tao Wu, email: wutao@ustc.edu.cn; XianHui Chen, email: chenxh@ustc.edu.cn)
†These authors contributed equally to this work.

1 Introduction

In recent decades, the exotic electronic states in kagome lattice, which holds a particular geometric frustration, have stimulated considerable interest and become a new frontier in condensed matter physics [1-21]. In contrast to the firm coupling limit at half-filling [1,2], the exploration of correlated electronic states in kagome lattice with intermediate coupling is still limited [3-5]. Although some intriguing electronic orders (such as chiral *d*-wave/*f*-wave superconductivity) have been theoretically proposed for the kagome Hubbard model [3-5], their experimental realization remains unclear in the kagome materials, particularly for exotic superconductivity. Recently, the discovery of superconductivity in vanadium-based kagome metal AV_3Sb_5 (A = K, Rb, Cs) with the maximum superconducting temperature $T_c \sim 3$ K has attracted considerable attention in the academic community [22-25], which provides a fertile playground to explore the correlation-driven exotic electronic states in kagome lattice.

Apart from superconductivity, a density-wave-like transition has been observed in these kagome metals with a transition temperature (T_s) ranging from 78 to 104 K [22]. Earlier X-ray scattering experiment has observed an in-plane translational symmetry breaking with a $2a \times 2a$ period below T_s, indicating a possible charge-density-wave (CDW) order [23]. Subsequently, scanning tunneling microscopy (STM) experiments have observed a $2a \times 2a$ charge modulation with a novel chiral anisotropy in KV_3Sb_5 [26]. In addition, recent STM and X-ray experiments have identified a three-dimensional (3D) charge modulation with a $2a \times 2a \times 2c$ period in CsV_3Sb_5 [27,28]. Theoretically, density functional theory calculation also confirms a 3D CDW state and suggests a Peierls-instability-driven CDW picture [29]. Meanwhile, a chiral flux phase has been proposed as the possible ground state instead of the $2a \times 2a$ charge order [30], in which time-reversal symmetry should be broken. Apart from the in-plane $2a \times 2a$ charge order, an additional $4a$ unidirectional charge order has been observed on the surface by STM experiments in CsV_3Sb_5 [31,32], whose underlying mechanism is still elusive. Furthermore, the interplay of superconductivity with CDW order has been explored by utilizing a high-pressure technique in CsV_3Sb_5 [33-37]. Different from the usual competing phase diagram between superconductivity and CDW order, the pressure-dependent T_c in CsV_3Sb_5 exhibits a nonmonotonic behavior, whereas the density-wave-like transition is continuously suppressed with increasing pressure below 2 GPa [34], indicating an unusual interplay between superconductivity and CDW order. In addition to the abovementioned CDW ordering below T_s, a possible orbital order may emerge in this system below T_s. In general, given the coupling between the orbital and lattice degrees of freedom, orbital ordering would inevitably lead to a structural phase transition [38]. In these new kagome superconductors AV_3Sb_5, considering a distorted octahedral crystal field on vanadium (V) sites caused by six anionic coordination atoms (Figure 1(a)) and actual $3d$ electron filling, nearly degenerate $3d$ orbitals can be held in the ground state after crystal field splitting, which allows for a possible orbital ordering below T_s [39]. Whether orbital ordering is really involved in the density-wave-like transition deserves further investigation. Here, we performed ^{51}V and ^{133}Cs nuclear magnetic resonance (NMR) measurements on a CsV_3Sb_5 single crystal to clarify the exact nature of density-wave-like transition in these kagome superconductors. The density-wave-like transition is clarified as a first-order structural transition with a 3D structural modulation. By measuring the angle-dependent full NMR spectrum and nuclear spin-lattice relaxation rate ($1/T_1$), the orbital order is considered as the primary electronic order induced by the first-order structural transition. Moreover, the evidence for possible orbital fluctuations is also revealed above T_s. The present work suggests rich orbital physics in these kagome superconductors.

2 Experimental methods

A commercial NMR spectrometer (Thamway Co., Ltd.) was used for NMR measurements. A magnet from Oxford Instruments, which can provide a uniform magnetic field up to 12 T, was used. The external magnetic field was calibrated by ^{63}Cu NMR with the sample coil. All NMR spectra were acquired by a standard spin-echo method with an FFT sum. For ^{51}V and ^{133}Cs, their nuclear spin number is $I = 7/2$, and their gyromagnetic ratio γ_N is 11.193 and 5.5844 MHz/T, respectively. In principle, their NMR spectra will split into a single central peak and six satellites under a strong magnetic field because of the nuclear quadrupole interaction. Considering only the first-order perturbation of quadrupole interaction, the resonance frequency of all transition lines are satisfied as follows [40]:

$$\begin{aligned} \nu &= \nu_0 + \nu_{m,m-1}^{(1)} \\ &= \nu_0 + \frac{1}{2}\nu_Q\left(m-\frac{1}{2}\right)\times(3\cos^2\theta - 1 - \eta\sin^2\theta\cos 2\phi), \end{aligned} \tag{1}$$

where ν_0 is the Larmor frequency of central peak; $\nu_Q = \frac{3eQV_{zz}}{2I(2I-1)\hbar}$ is the quadrupole frequency in the z principal axis of the electric field gradient (EFG) tensor; m is the z-axis spin number; θ and ϕ are the Euler angles between external field H_0 and the principal axis of the EFG tensor; η is the asymmetry parameter, defined as $\eta = \left|\frac{V_{xx}-V_{yy}}{V_{zz}}\right|$, where $|V_{xx}| \le |V_{yy}| \le |V_{zz}|$ are the three principal components of the EFG tensor. This equation can be used to calculate the fre-

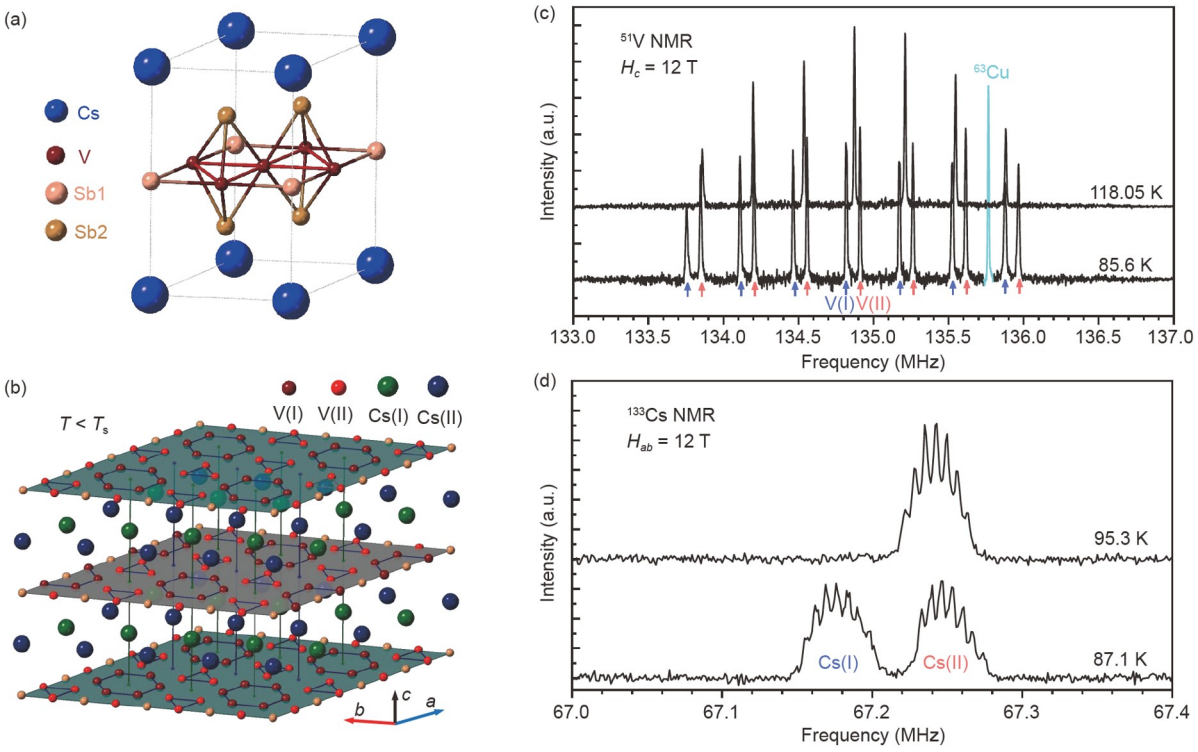

Figure 1 (Color online) 3D structural modulation by ^{51}V and ^{133}Cs NMR. (a) Crystal structure of CsV_3Sb_5 above T_s; (b) illustration of $2a \times 2a \times 2c$ modulation with different V/Cs sites and inverse Star of David structure in kagome lattice below T_s; (c) the representative ^{51}V NMR spectra measured above and below T_s with the external magnetic field $H = 12$ T along the c axis (H_c); (d) the representative ^{133}Cs NMR spectra measured above and below T_s with $H = 12$ T parallel to the ab plane (H_{ab}). The present NMR spectrum indicates that two inequivalent V and Cs sites are found below T_s, which are labeled as V(I), V(II) and Cs(I), Cs(II), respectively.

quency interval between adjacent m, which is $\left|\frac{1}{2}\nu_Q(3\cos^2\theta - 1 - \eta\sin^2\theta\cos 2\phi)\right|$ corresponding to the frequency interval of adjacent peaks in the NMR spectrum. All ν_Q data were determined as the average frequency interval of adjacent peaks. The measurement of spin-lattice relaxation time T_1 used the inversed pulse method and saturated pulse method for ^{51}V and ^{133}Cs, respectively. The relaxation curve was measured in the central peak of the ^{51}V spectrum and fitted by [40]

$$m(t) = m_0 + m_1\left[\frac{1}{84}e^{-\left(\frac{t}{T_1}\right)^r} + \frac{3}{44}e^{-\left(\frac{6t}{T_1}\right)^r} + \frac{75}{364}e^{-\left(\frac{15t}{T_1}\right)^r} + \frac{1225}{1716}e^{-\left(\frac{28t}{T_1}\right)^r}\right], \quad (2)$$

where r is the inhomogeneous parameter. In the case of ^{133}Cs, the central peak and all satellites were excited simultaneously; thus, the fitting function was simplified as follows:

$$m(t) = m_0 + m_1 e^{-\left(\frac{t}{T_1}\right)^r}. \quad (3)$$

3 Results and discussion

As shown in Figure 1(a), the sublattice consisting of V atoms forms an intriguing two-dimensional (2D) kagome net, in which each V atom has six antimony (Sb) atoms as anionic coordination. The six coordinating Sb atoms can be further divided into two kinds of Sb sites at the high-temperature structural phase, including two in-plane Sb(1) sites and four out-of-plane Sb(2) sites. The cesium (Cs) atoms are on the top of Sb(1) sites, and they individually form an isolating layer between two neighboring $[V_3Sb_5]^-$ layers. Cs^+ layers and $[V_3Sb_5]^-$ layers are alternatively stacked along the c axis, forming a layered structure with the space group of $P6/mmm$ [22]. In principle, NMR spectra are sensitive to the change of local structural environment around the measured nuclei. Here, we performed NMR measurements on ^{51}V and ^{133}Cs nuclei, both of which the nuclear spin number (I) is 7/2. Given the electric quadrupole interaction between nuclei with $I > 1/2$ and electrons, the single NMR spectrum of high-spin nuclei would split into $2I$ transition lines separated by a quadrupole frequency ($\upsilon_{\alpha\alpha}$). As shown in Figure 1(c) and (d), the high-temperature NMR spectra of ^{51}V and ^{133}Cs only have one set of NMR transition lines with $2I$ equally separated peaks, which is consistent with only one structural site for V and Cs sublattices above T_s (Figure 1(a)). Below T_s, the NMR spectra of both ^{51}V and ^{133}Cs split into two sets of NMR transition lines, indicating the two distinct structural sites for V and Cs sublattices. Considering a first-order ap-

proximation, the NMR spectrum of ^{51}V would be only sensitive to the in-plane structural modulation. By contrast, apart from in-plane modulation, the NMR spectrum of interlaminar ^{133}Cs is dependent on the structural modulation along the *c* axis. Based on previous STM and X-ray scattering experiments [27,28], the density-wave-like transition leads to a 3D structural modulation with a $2a \times 2a \times 2c$ period. Based on NMR spectral analysis, both NMR spectra of ^{51}V and ^{133}Cs should split into two sets of transition lines with equal spectral weight (see details in sect. S3 of Supplementary Materials). This finding is consistent with our present observations, which supports a $2a \times 2a \times 2c$ period in bulk CsV_3Sb_5. Notably, our result of ^{133}Cs NMR only puts a constrain with a π-phase shift between two neighboring layers to the 3D structural modulation, which is not necessary for calculating $2a \times 2a \times 2c$. Recently, a new 3D structural modulation with a $2a \times 2a \times 4c$ period has also been observed in X-ray scattering experiments on CsV_3Sb_5 [41]. Our present NMR results cannot distinguish the difference between $2a \times 2a \times 2c$ and $2a \times 2a \times 4c$.

Next, we will discuss the origin of the observed NMR splitting at ^{51}V nuclei. In general, the magnetic and quadrupole interaction between nuclei and electrons can produce the splitting in the NMR spectrum below T_s. However, they would give different manifestations in the NMR spectrum. As shown in Figure 1(c), the splitting on each NMR transition line is almost the same, which indicates that the predominant contribution of splitting is not from the quadrupole interaction but magnetic interaction. We measured the splitting in great detail to extract the temperature dependence of the magnetic splitting on the central transition lines. As shown in Figure 2(a), the temperature-dependent central transition lines show a typical behavior for a first-order phase transition, which holds a narrow temperature range of approximately 2 K to exhibit two-phase coexistence. Moreover, the splitting of the NMR spectra shows a sudden jump at T_s, which is consistent with a first-order phase transition. The same results were confirmed by a recent NMR work on CsV_3Sb_5 [42]. In supplementary materials, we also measure the field dependence of splitting (see details in sect. S6 of Supplementary Materials), indicating that such magnetic splitting comes from a splitting of the Knight shift instead of a spontaneous internal field. Therefore, time-reversal symmetry is still preserved below T_s. This result is also consistent with the previous μSR experiment [43]. The temperature-dependent splitting of the Knight shift is plotted in Figure 2(b). After a sudden jump at T_s, the splitting shows a continuous increase and finally becomes saturated at low temperatures below 20 K.

Now the question is how to understand the sudden change of the Knight shift at T_s. In principle, the Knight shift has two major contributions, including spin shift (K_{spin}) and orbital shift (K_{orb}). The spin shift is proportional to spin susceptibility (χ_{spin}), and the orbital shift is proportional to orbital susceptibility (χ_{orb}). Here, the major splitting of the Knight shift is ascribed to the orbital shift (a major splitting caused by the orbital shift is also confirmed in ^{133}Cs NMR, which is shown in sect. S3 of Supplementary Materials), suggesting a possible change in crystal field or orbital state below T_s. In general, the orbital momentum is quenched under the crystal field, and then the orbital susceptibility is primarily related to the Van Vleck orbital paramagnetism, which is proportional

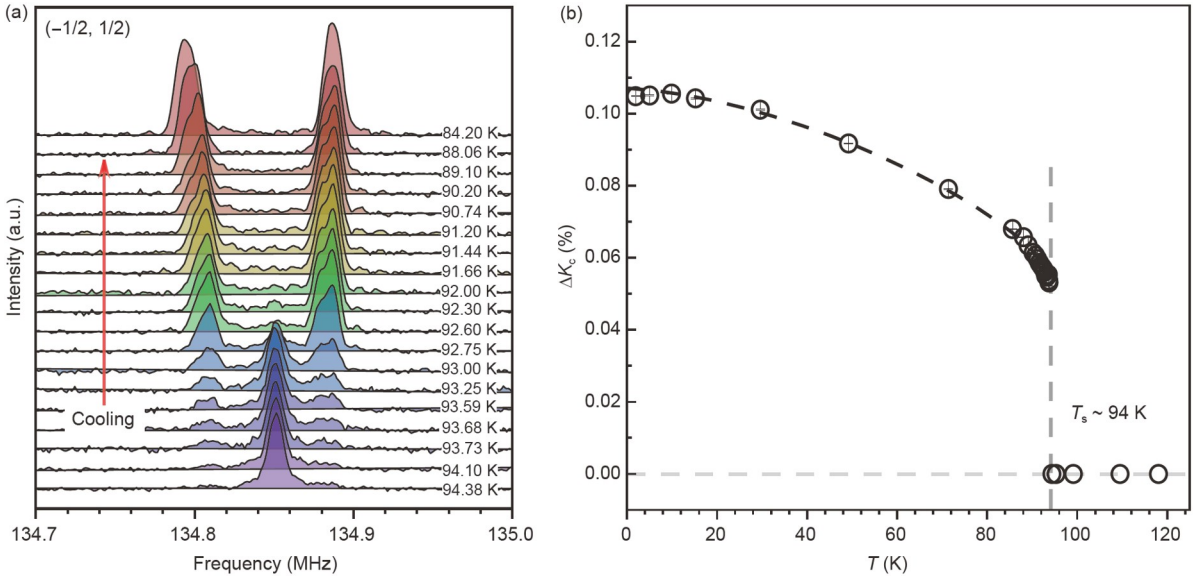

Figure 2 (Color online) First-order phase transition associated with orbital ordering by ^{51}V NMR. (a) Temperature dependence of the central transition lines of ^{51}V NMR with temperature cooling across T_s; (b) temperature dependence of the splitting of Knight shift (ΔK_c), which is obtained by calculating the difference of Knight shift between V(I) and V(II) sites. The coexistence of high-temperature and low-temperature phases between 92 and 94.38 K. A sudden jump of ΔK_c manifests a first-order phase transition associated with an orbital ordering at T_s.

to $1/\Delta$ [39], where Δ is the energy gap between the ground state and excited states under a certain crystal field. The energy scale of Δ in 3*d* transition metal can vary in a wide range of energy scales from ~0.1 to ~1 eV [39,44,45]. The change in the local structural environment could lead to a corresponding change in local Δ at different sites. Therefore, a slight change of orbital shift is expected across a structural phase transition. However, the orbital order is beyond such a trivial situation, leading to a reconstruction of orbital states similar to those in manganites [38]. In this study, the magnitude of the observed splitting from the orbital shift is high, which is close to one-third of the total Knight shift, and it is hard to explain using a weak structural phase transition without reconstruction of orbital states or a change of orbital population [44,45]. Therefore, the large splitting of the orbital shift suggests a possible orbital ordering at T_s. Next, we will show more evidences for orbital ordering by measuring the anisotropy of the Knight shift and $1/T_1T$.

As shown in Figure 3, we systematically measure the temperature-dependent Knight shift and spin-lattice relaxation rate ($1/T_1$) under an external magnetic field along three principal axes (*X*, *Y*, and *Z*) of local EFG around ^{51}V nuclei. Notably, the Knight shift and $1/T_1T$ of ^{51}V nuclei show distinct temperature-dependent behavior above T_s. For a Fermi liquid, K_{spin} and $1/T_1T$ hold a standard Korringa relation with $1/T_1T$–K^2_{spin}. In this study, K_{spin} at ^{51}V nuclei can be ascribed to two kinds of magnetic hyperfine interaction, including core polarization effect and magnetic dipole-dipole interaction. In addition, the anisotropy of K_{spin} is determined by the magnetic dipole-dipole interaction, which usually depends on the occupation of orbital states [46-50]. If the temperature-dependent Knight shift primarily comes from K_{spin}, then the nearly isotropic temperature-dependent part above T_s indicates that the core polarization effect is the predominant

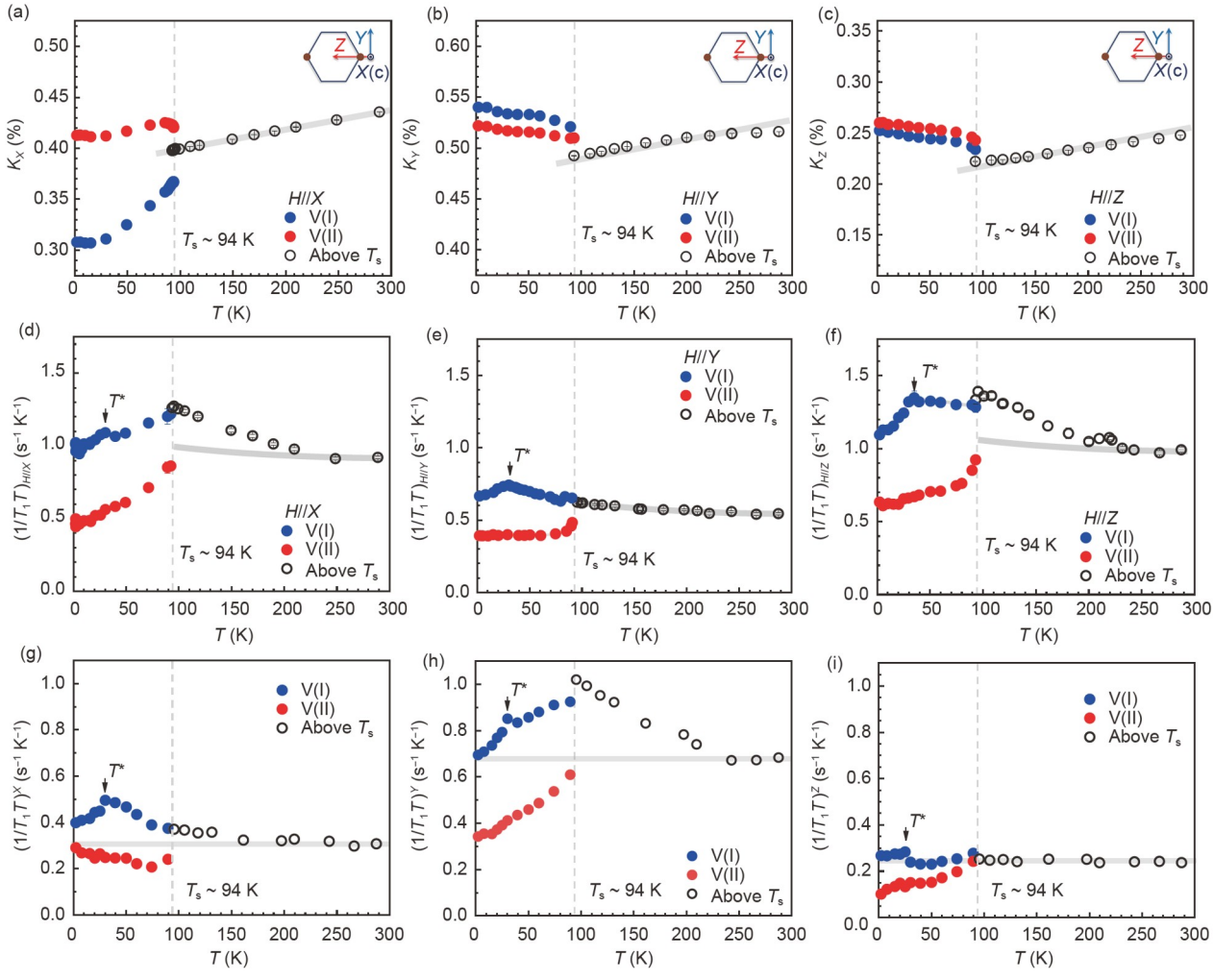

Figure 3 (Color online) Temperature-dependent Knight shift and $1/T_1T$ under the external magnetic field along the principal axes. (a)-(c) Temperature-dependent Knight shift with the external magnetic *H* parallel to the *X*, *Y*, and *Z* axes. Insert: sketch of the principal coordinate system of EFG, in which the crystal *c* axis is chosen as the *X* axis. (d)-(f) Temperature-dependence of $1/T_1T$ with the external magnetic *H* parallel to the *X*, *Y*, and *Z* axes. The gray dash lines are a guide for the eye for the critical temperature T_s. (g)-(i) Temperature-dependent fluctuating hyperfine fields along the *X*, *Y*, and *Z* axes. $(1/T_1T)_{H//Z}$ is the sum of contribution from transverse fluctuating hyperfine fields ($(1/T_1T)^X$, $(1/T_1T)^Y$) with $(1/T_1T)_{H//Z} = (1/T_1T)^X + (1/T_1T)^Y$. Following this relation, we could extract $(1/T_1T)^\alpha$ by a linear combination of $(1/T_1T)_{H//\alpha}$ (α = *X*, *Y*, *Z*).

magnetic hyperfine interaction. Then, we would expect a similar isotropic temperature-dependent $1/T_1T$. However, this is inconsistent with our present observation in $1/T_1T$. As shown in Figure 3(d)-(f), the temperature-dependent $1/T_1T$ shows a clear anisotropy above T_s. On the contrary, similar to most metals, an almost temperature-independent spin susceptibility is expected in our case, which is inferred from the results of recent STM experiments [26,27]. Therefore, the temperature-dependence of Knight shift should be ascribed to K_{orb} instead of K_{spin}. Furthermore, the temperature dependence of the Knight shift at ^{51}V sites is consistent with that of bulk susceptibility above T_s (see the temperature-dependent bulk susceptibility in sect. S1 of Supplementary Materials), supporting a temperature-dependent χ_{orb}.

How to understand the anisotropic $1/T_1T$ above T_s? In general, $1/T_1T$ measures the transverse fluctuating hyperfine fields, and it can be phenomenologically divided into two kinds of contribution with $1/T_1T = (1/T_1T)_{FL} + (1/T_1T)_{SF}$, where $(1/T_1T)_{FL}$ is related to the fluctuating hyperfine fields following Fermi liquid behavior. In addition, $(1/T_1T)_{SF}$ is related to the additional fluctuating hyperfine fields. Considering the temperature-independent spin susceptibility, temperature-dependent $1/T_1T$ suggests a significant contribution from fluctuating hyperfine fields beyond a Fermi liquid. As shown in Figure 3(g)-(i), each component of the fluctuating hyperfine field along the X, Y, and Z axes can be extracted by a linear combination of $(1/T_1T)_{H//\alpha}$ ($\alpha = X, Y, Z$). Notably, the $(1/T_1T)_{SF}$ is primarily originated from the fluctuating hyperfine field along the Y direction. By contrast, the fluctuating hyperfine field along the Z direction shows a temperature-independent behavior, which is quite consistent with temperature-independent spin susceptibility. The additional fluctuating hyperfine fields along the Y direction are related to orbital fluctuations above T_s. Notably, such additional fluctuating hyperfine fields caused by orbital fluctuations are not found in $1/T_1T$ of ^{133}Cs, indicating the major orbital fluctuations from the orbitals at V sites (see details in sect. S3 of Supplementary Materials). Below T_s, a sudden jump also appears in the fluctuating hyperfine field along the Y direction but not the Z direction, indicating the possible suppression of orbital fluctuations caused by orbital ordering. The missing jump for the fluctuating hyperfine field along the Z direction indicates that the jump of the Knight shift at T_s is related to the orbital shift instead of the spin shift. By monitoring the fluctuating hyperfine field along the Z direction below T_s, we found that only V(I) sites exhibit a clear reduction of the density of states at Fermi energy, which is also supported by the ^{133}Cs NMR results (see details in sect. S3 of Supplementary Materials). This finding is entirely consistent with a CDW gap observed by STM and angle-resolved photoemission spectroscopic (ARPES) experiments [26,27,51].

Below T_s, the distinct temperature dependence of the Knight shift among different magnetic field directions at V(I) sites indicates orbital ordering. As discussed above, the temperature dependence of the Knight shift is primarily related to the orbital shift, which exhibits the same temperature-dependent behavior along all directions above T_s. Below T_s, if we only consider a simple change of Δ caused by a crystal field, then the temperature dependence of the orbital shift should also exhibit the same temperature-dependent behavior along all directions. Therefore, the anisotropic temperature dependence of the Knight shift below T_s at V(I) is beyond a simple change of crystal field, which suggests a reconstruction of orbital states. By contrast, no significant reconstruction of orbital states is found at V(II) sites because of a nearly isotropic change of orbital shift below T_s. Apart from the orbital shift, the EFG parameters also indicate orbital ordering. In general, the charging order and orbital order can affect the EFG parameters [52,53]. As shown in Figure 4, the temperature-dependent quadrupole frequency (ν_Q) and asymmetry parameter (η) are also extracted from the

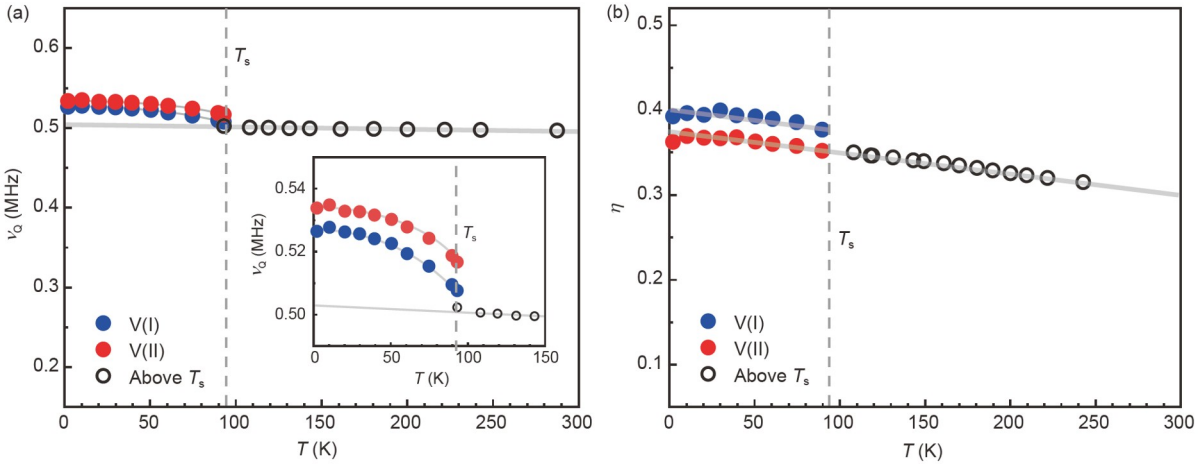

Figure 4 (Color online) Temperature-dependent EFG parameters. (a) Temperature-dependent quadrupole frequency (ν_Q); (b) temperature-dependent asymmetry parameter (η).

full NMR spectrum along the three principal axes of the EFG tensor. The comprehensive effect from the change of crystal field, orbital order, and CDW order below T_s leads to the same behavior of ν_Q at both V(I) and V(II) sites. However, the temperature-dependent asymmetry parameter shows a sudden jump below T_s only for V(I) sites, which is also consistent with the reconstruction of orbital states at V(I) sites. Considering the structural distortion in the proposed inverse Star of David (or Star of David) superlattice model [29], our results suggest that the orbital states of V sites in the triangle and hexagonal vanadium clusters are quite different. These results are similar to the orbital ordering caused by vanadium trimerization in $LiVO_2$ [48]. Thus, a large Van Vleck orbital susceptibility is observed, and the Knight shift and EFG parameters are affected by the orbital order. Furthermore, the recent ARPES experiment suggests a significant reconstruction of the band structure below T_s, which is beyond a simple Fermi surface nesting picture [54].

4 Conclusions

To date, our NMR results demonstrate the rich orbital physics in CsV_3Sb_5, including orbital order and relevant orbital fluctuations. However, the exact orbital physics needs more theoretical inputs on these new kagome superconductors to achieve a comprehensive understanding. In addition, the correlation between orbital ordering/fluctuations and superconductivity must be explored in this system. Based on previous high-pressure studies on CsV_3Sb_5, superconductivity could be enhanced, and the transition temperature could reach a maximum when the density-wave-like transition is completely suppressed around 2.0 GPa [33,34]. Our present NMR results indicate that the orbital fluctuations might also be enhanced around this critical pressure. Whether the optimized superconductivity is related to a possible enhancement of orbital fluctuations deserves further exploration. In addition, an unconventional chiral charge order with chiral anisotropy has been observed by previous STM experiments [26]. Based on the present NMR results, the observed orbital order and secondary CDW order only break the translational symmetry and not the rotational symmetry. If the rotational symmetry is broken at low temperatures as suggested by the STM results, then a nematic phase transition below T_s would be expected. In fact, the temperature-dependent $1/T_1T$ shows kink behavior around T^*~35 K, indicating a possible phase transition related to rotational symmetry breaking. Conducting more experiments are desired in the future to uncover the possible nematic phase transition.

This work was supported by the National Key R&D Program of China (Grant Nos. 2017YFA0303000, and 2016YFA0300201), the National Natural Science Foundation of China (Grant Nos. 11888101, and 12034004), the Strategic Priority Research Program of the Chinese Academy of Sciences (Grant No. XDB25000000), the Anhui Initiative in Quantum Information Technologies (Grant No. AHY160000), and the Collaborative Innovation Program of Hefei Science Center, CAS (Grant No. 2019HSC-CIP007). We thank the valuable discussion with YiLin Wang, Gang Chen, and JunFeng He.

Supporting Information

The supporting information is available online at http://phys.scichina.com and https://link.springer.com. The supporting materials are published as submitted, without typesetting or editing. The responsibility for scientific accuracy and content remains entirely with the authors.

1 Y. Ran, M. Hermele, P. A. Lee, and X. G. Wen, Phys. Rev. Lett. **98**, 117205 (2007).
2 W. H. Ko, P. A. Lee, and X. G. Wen, Phys. Rev. B **79**, 214502 (2009).
3 S. L. Yu, and J. X. Li, Phys. Rev. B **85**, 144402 (2012).
4 M. L. Kiesel, C. Platt, and R. Thomale, Phys. Rev. Lett. **110**, 126405 (2013).
5 W. S. Wang, Z. Z. Li, Y. Y. Xiang, and Q. H. Wang, Phys. Rev. B **87**, 115135 (2013).
6 J. Wen, A. Rüegg, C. C. J. Wang, and G. A. Fiete, Phys. Rev. B **82**, 075125 (2010).
7 S. Nakatsuji, N. Kiyohara, and T. Higo, Nature **527**, 212 (2015).
8 K. Kuroda, T. Tomita, M. T. Suzuki, C. Bareille, A. A. Nugroho, P. Goswami, M. Ochi, M. Ikhlas, M. Nakayama, S. Akebi, R. Noguchi, R. Ishii, N. Inami, K. Ono, H. Kumigashira, A. Varykhalov, T. Muro, T. Koretsune, R. Arita, S. Shin, T. Kondo, and S. Nakatsuji, Nat. Mater. **16**, 1090 (2017).
9 L. Ye, M. Kang, J. Liu, F. von Cube, C. R. Wicker, T. Suzuki, C. Jozwiak, A. Bostwick, E. Rotenberg, D. C. Bell, L. Fu, R. Comin, and J. G. Checkelsky, Nature **555**, 638 (2018).
10 E. Liu, Y. Sun, N. Kumar, L. Muechler, A. Sun, L. Jiao, S. Y. Yang, D. Liu, A. Liang, Q. Xu, J. Kroder, V. Süß, H. Borrmann, C. Shekhar, Z. Wang, C. Xi, W. Wang, W. Schnelle, S. Wirth, Y. Chen, S. T. B. Goennenwein, and C. Felser, Nat. Phys. **14**, 1125 (2018).
11 J. X. Yin, S. S. Zhang, H. Li, K. Jiang, G. Chang, B. Zhang, B. Lian, C. Xiang, I. Belopolski, H. Zheng, T. A. Cochran, S. Y. Xu, G. Bian, K. Liu, T. R. Chang, H. Lin, Z. Y. Lu, Z. Wang, S. Jia, W. Wang, and M. Z. Hasan, Nature **562**, 91 (2018).
12 Q. Wang, Y. Xu, R. Lou, Z. Liu, M. Li, Y. Huang, D. Shen, H. Weng, S. Wang, and H. Lei, Nat. Commun. **9**, 3681 (2018).
13 Z. Lin, J. H. Choi, Q. Zhang, W. Qin, S. Yi, P. Wang, L. Li, Y. Wang, H. Zhang, Z. Sun, L. Wei, S. Zhang, T. Guo, Q. Lu, J. H. Cho, C. Zeng, and Z. Zhang, Phys. Rev. Lett. **121**, 096401 (2018).
14 M. Kang, L. Ye, S. Fang, J. S. You, A. Levitan, M. Han, J. I. Facio, C. Jozwiak, A. Bostwick, E. Rotenberg, M. K. Chan, R. D. McDonald, D. Graf, K. Kaznatcheev, E. Vescovo, D. C. Bell, E. Kaxiras, J. van den Brink, M. Richter, M. Prasad Ghimire, J. G. Checkelsky, and R. Comin, Nat. Mater. **19**, 163 (2020).
15 J. X. Yin, W. Ma, T. A. Cochran, X. Xu, S. S. Zhang, H. J. Tien, N. Shumiya, G. Cheng, K. Jiang, B. Lian, Z. Song, G. Chang, I. Belopolski, D. Multer, M. Litskevich, Z. J. Cheng, X. P. Yang, B. Swidler, H. Zhou, H. Lin, T. Neupert, Z. Wang, N. Yao, T. R. Chang, S. Jia, and M. Zahid Hasan, Nature **583**, 533 (2020).
16 Y. Xing, J. Shen, H. Chen, L. Huang, Y. Gao, Q. Zheng, Y. Y. Zhang, G. Li, B. Hu, G. Qian, L. Cao, X. Zhang, P. Fan, R. Ma, Q. Wang, Q. Yin, H. Lei, W. Ji, S. Du, H. Yang, W. Wang, C. Shen, X. Lin, E. Liu, B. Shen, Z. Wang, and H. J. Gao, Nat. Commun. **11**, 5613 (2020).
17 H. M. Guo, and M. Franz, Phys. Rev. B **80**, 113102 (2009).
18 I. I. Mazin, H. O. Jeschke, F. Lechermann, H. Lee, M. Fink, R. Thomale, and R. Valentí, Nat. Commun. **5**, 4261 (2014).
19 D. F. Liu, A. J. Liang, E. K. Liu, Q. N. Xu, Y. W. Li, C. Chen, D. Pei,

W. J. Shi, S. K. Mo, P. Dudin, T. Kim, C. Cacho, G. Li, Y. Sun, L. X. Yang, Z. K. Liu, S. S. P. Parkin, C. Felser, and Y. L. Chen, Science **365**, 1282 (2019).
20 I. Belopolski, K. Manna, D. S. Sanchez, G. Chang, B. Ernst, J. Yin, S. S. Zhang, T. Cochran, N. Shumiya, H. Zheng, B. Singh, G. Bian, D. Multer, M. Litskevich, X. Zhou, S. M. Huang, B. Wang, T. R. Chang, S. Y. Xu, A. Bansil, C. Felser, H. Lin, and M. Z. Hasan, Science **365**, 1278 (2019).
21 N. Morali, R. Batabyal, P. K. Nag, E. Liu, Q. Xu, Y. Sun, B. Yan, C. Felser, N. Avraham, and H. Beidenkopf, Science **365**, 1286 (2019).
22 B. R. Ortiz, L. C. Gomes, J. R. Morey, M. Winiarski, M. Bordelon, J. S. Mangum, I. W. H. Oswald, J. A. Rodriguez-Rivera, J. R. Neilson, S. D. Wilson, E. Ertekin, T. M. McQueen, and E. S. Toberer, Phys. Rev. Mater. **3**, 094407 (2019).
23 B. R. Ortiz, S. M. L. Teicher, Y. Hu, J. L. Zuo, P. M. Sarte, E. C. Schueller, A. M. M. Abeykoon, M. J. Krogstad, S. Rosenkranz, R. Osborn, R. Seshadri, L. Balents, J. He, and S. D. Wilson, Phys. Rev. Lett. **125**, 247002 (2020).
24 B. R. Ortiz, P. M. Sarte, E. M. Kenney, M. J. Graf, S. M. L. Teicher, R. Seshadri, and S. D. Wilson, Phys. Rev. Mater. **5**, 034801 (2021).
25 Q. Yin, Z. Tu, C. Gong, Y. Fu, S. Yan, and H. Lei, Chin. Phys. Lett. **38**, 037403 (2021).
26 Y. X. Jiang, J. X. Yin, M. M. Denner, N. Shumiya, B. R. Ortiz, G. Xu, Z. Guguchia, J. He, M. S. Hossain, X. Liu, J. Ruff, L. Kautzsch, S. S. Zhang, G. Chang, I. Belopolski, Q. Zhang, T. A. Cochran, D. Multer, M. Litskevich, Z. J. Cheng, X. P. Yang, Z. Wang, R. Thomale, T. Neupert, S. D. Wilson, and M. Z. Hasan, Nat. Mater. **20**, 1353 (2021).
27 Z. Liang, X. Hou, F. Zhang, W. Ma, P. Wu, Z. Zhang, F. Yu, J. J. Ying, K. Jiang, L. Shan, Z. Wang, and X. H. Chen, Phys. Rev. X **11**, 031026 (2021).
28 H. Li, T. T. Zhang, T. Yilmaz, Y. Y. Pai, C. E. Marvinney, A. Said, Q. W. Yin, C. S. Gong, Z. J. Tu, E. Vescovo, C. S. Nelson, R. G. Moore, S. Murakami, H. C. Lei, H. N. Lee, B. J. Lawrie, and H. Miao, Phys. Rev. X **11**, 031050 (2021).
29 H. Tan, Y. Liu, Z. Wang, and B. Yan, Phys. Rev. Lett. **127**, 046401 (2021).
30 X. Feng, K. Jiang, Z. Wang, and J. Hu, Sci. Bull. **66**, 1384 (2021).
31 H. Zhao, H. Li, B. R. Ortiz, S. M. L. Teicher, T. Park, M. Ye, Z. Wang, L. Balents, S. D. Wilson, and I. Zeljkovic, arXiv: 2103.03118.
32 H. Chen, H. Yang, B. Hu, Z. Zhao, J. Yuan, Y. Xing, G. Qian, Z. Huang, G. Li, Y. Ye, S. Ma, S. Ni, H. Zhang, Q. Yin, C. Gong, Z. Tu, H. Lei, H. Tan, S. Zhou, C. Shen, X. Dong, B. Yan, Z. Wang, and H. J. Gao, Nature **599**, 222 (2021).
33 C. C. Zhao, L. S. Wang, W. Xia, Q. W. Yin, J. M. Ni, Y. Y. Huang, C. P. Tu, Z. C. Tao, Z. J. Tu, C. S. Gong, H. C. Lei, Y. F. Guo, X. F. Yang, and S. Y. Li, arXiv: 2102.08356.
34 K. Y. Chen, N. N. Wang, Q. W. Yin, Y. H. Gu, K. Jiang, Z. J. Tu, C. S. Gong, Y. Uwatoko, J. P. Sun, H. C. Lei, J. P. Hu, and J. G. Cheng, Phys. Rev. Lett. **126**, 247001 (2021).
35 X. Chen, X. Zhan, X. Wang, J. Deng, X. B. Liu, X. Chen, J. G. Guo, and X. Chen, Chin. Phys. Lett. **38**, 057402 (2021).
36 Z. Zhang, Z. Chen, Y. Zhou, Y. Yuan, S. Wang, J. Wang, H. Yang, C. An, L. Zhang, X. Zhu, Y. Zhou, X. Chen, J. Zhou, and Z. Yang, Phys. Rev. B **103**, 224513 (2021).
37 F. Du, S. Luo, B. R. Ortiz, Y. Chen, W. Duan, D. Zhang, X. Lu, S. D. Wilson, Y. Song, and H. Yuan, Phys. Rev. B **103**, L220504 (2021).
38 Y. Tokura, and N. Nagaosa, Science **288**, 462 (2000).
39 S. V. Streltsov, and D. I. Khomskii, Phys.-Uspekhi **60**, 1121 (2017).
40 P. P. Man, in *Quadrupole Interaction*: *Encyclopedia of Nuclear Magnetic Resonance Vol. 6*, edited by D. M. Grant, and R. K. Harris (John Wiley and Sons, Chichester, 1996), pp. 3838-3848.
41 B. R. Ortiz, S. M. L. Teicher, L. Kautzsch, P. M. Sarte, N. Ratcliff, J. Harter, J. P. C. Ruff, R. Seshadri, and S. D. Wilson, Phys. Rev. X **11**, 041030 (2021).
42 C. Mu, Q. Yin, Z. Tu, C. Gong, H. Lei, Z. Li, and J. Luo, Chin. Phys. Lett. **38**, 077402 (2021).
43 E. M. Kenney, B. R. Ortiz, C. Wang, S. D. Wilson, and M. J. Graf, J. Phys.-Condens. Matter **33**, 235801 (2021).
44 P. D. Johnson, G. Xu, and W. G. Yin, *Iron-based Superconductivity*, *Vol. 211* (Springer, Berlin, 2015).
45 W. E. Pickett, Rev. Mod. Phys. **61**, 433 (1989).
46 T. Kiyama, T. Shiraoka, M. Itoh, L. Kano, H. Ichikawa, and J. Akimitsu, Phys. Rev. B **73**, 184422 (2006).
47 T. Suzuki, I. Yamauchi, M. Itoh, T. Yamauchi, and Y. Ueda, Phys. Rev. B **73**, 224421 (2006).
48 T. Jin-no, Y. Shimizu, M. Itoh, S. Niitaka, and H. Takagi, Phys. Rev. B **87**, 075135 (2013).
49 Y. Shimizu, S. Aoyama, T. Jinno, M. Itoh, and Y. Ueda, Phys. Rev. Lett. **114**, 166403 (2015).
50 I. Yamauchi, M. Itoh, T. Yamauchi, J. I. Yamaura, and Y. Ueda, Phys. Rev. B **96**, 205114 (2017).
51 Z. Wang, S. Ma, Y. Zhang, H. Yang, Z. Zhao, Y. Ou, Y. Zhu, S. Ni, Z. Lu, H. Chen, K. Jiang, L. Yu, Y. Zhang, X. Dong, J. P. Hu, H. J. Gao, and Z. X Zhao, arXiv: 2104.05556.
52 D. W. Song, J. Li, D. Zhao, L. K. Ma, L. X. Zheng, S. J. Li, L. P. Nie, X. G. Luo, Z. P. Yin, T. Wu, and X. H. Chen, Phys. Rev. B **98**, 235142 (2018).
53 T. Wu, H. Mayaffre, S. Krämer, M. Horvatić, C. Berthier, W. N. Hardy, R. Liang, D. A. Bonn, and M. H. Julien, Nature **477**, 191 (2011).
54 Y. Hu, S. M. Teicher, B. R. Ortiz, Y. Luo, S. Peng, L. Huai, J. Z. Ma, N. C. Plumb, S. D. Wilson, J. F. He, and M. Shi, arXiv: 2104.12725.